Chapter 2

Overview of Coandă MAV as an Aerial Robotic Platform

Harijono Djojodihardjo

Additional information is available at the end of the chapter

http://dx.doi.org/10.5772/intechopen.70157

Abstract

With the increasing need of micro-air-vehicles (MAVs) and advances in MAV technology, Coandă MAVs offer new promises and challenges. In this context, Coandă MAVs capabilities are analyzed. As a baseline, a mathematical model for a spherical Coandă MAV in hover and translatory motion is developed and analyzed from first physical principles. A computational fluid dynamic (CFD) simulations for a Coandă MAV generic model are carried out to assess the theoretical prediction and obtaining further physical insight on the Coandă MAV flow physics. The mathematical model and performance measures are developed to assess the capability of the semi-spherical Coandă MAV in performing effective flight as an aerial robotic platform, as indicated by the relationships between the relevant parameters of the mathematical model of the Coandă MAV to its system of flight forces.

Keywords: aerial robot, Coandă micro air vehicle (CMAV), Coandă MAV aerodynamics, Coandă MAV flight dynamics, unmanned micro air vehicle (UMAV)

Subject Area: Aerodynamics, Aerospace Engineering, Applied Mathematics and Physics, Flight Mechanics

1. Introduction

The utilization of Coandă effect and Coandă jet [1, 2] for flight vehicles have been carried out for a range of aircrafts and vehicles for decades and for future aircrafts [3–14], due to its flow control effectiveness. Other applications are potential in wind-turbines technology [15–20], and the Coanda effect have also been found and utilized in many other engineering applications and health science, such as in the upper respiratory system [20–24]. The science of flow control can be considered to originate from Prandtl [25] seminal paper in 1904, which has been hailed as a breakthrough in the science of fluid mechanics by the introduction of the boundary-layer theory. Prandtl's theory can be accounted for the physics of the separation phenomena and the boundary layers control.

The Coandă effect is based on the property of a jet flow to attach itself to a curved surface as it tangentially blows along and to remain attached until it leaves the surface or reach a critical stability breakdown. Coandă jet is one of the flow control techniques for modifying and enhancing aerodynamic performance, stability and control. Coandă jet has also been applied in the development of novel aircrafts for short take-off and landing. With the progress of many enabling technologies and need for disaster mitigation, security, and environmental conservation, the relatively new application of Coandă effect in micro-air-vehicles (MAVs) as robotic platforms is very challenging. Capitalizing on the basic fundamental principles, the aero- and flight dynamics of a baseline Coandă MAV configuration are analyzed and developed to formulate the relationships between various essential parameters to the equation of motion in hover, and translatory motion, which should give further insight on and can be further elaborated into other Coandă MAV characteristics and performance related to maneuver and stability and control.

Coandă micro-air-vehicles have been developed in various configurations. To meet the desired Coandă MAV operation, mission, and design requirements, one should establish the basic working relationships among various significant design parameters and variables to the generated aerodynamics forces. For this purpose, several approaches can be followed. The most logical first approach is the analytical tool based on basic fundamental principles. With the impressive progress of computational fluid dynamics (CFD) which has brought with it flow visualization capabilities; CFD utilization will assist the identification to the problem and assessment of the analytical approach. Furthermore, CFD visualization facilitates better insight and identification of salient details. Another important approach is the use of experimental tools, which is the foundation of scientific observation through meticulous experimental design and has intricate relationships with analytical approach. For the conceptual and prototype design stages, analytical, and CFD computational and visualization tools will expedite the efforts to that end.

The theoretical analysis, mathematical modeling and synthesis or Coandă micro-air-vehicles as an aerial robot platform will start with the identification and definition of a Coandă jet as a relatively thin and slightly viscous jet flowing over and adhere on a smooth curved surface. The main physical parameters are the angle of separation, θ; slot width, b; radius of curvature, R; Reynolds number, Re; the Coandă jet velocity, pressure differential $p_s - p_\infty$, Reynolds number and the Coandă jet momentum coefficient. Various platforms will be discussed to define the merit of Coandă MAV as a robotic platform. Hovering semi-spherical Coandă MAV will be utilized in the baseline aerodynamic analysis. The mathematical model of Coandă MAV to generate the equation of motion starts with first principles and the basic flight dynamic equation. CFD simulation and demonstration experiment are elaborated to assess the functionality of Coandă MAV aerial robot platform.

In the model development and analysis of a semi-spherical Coandă MAV, a propulsion system is utilized to introduce a Coandă jet blanket which is deflected downward due to the curved upper surface of the vehicle, to provide both hover as well as cruise capabilities. Such Coandă jet has been utilized for circulation enhancement for fixed-wing aircraft in forward flight and turbine blades movement [4–9, 12–20]. Thus, lift will be generated [27–35], which can be

utilized for hover and later for cruise propulsion [10, 35, 36]. The principle of Coandă MAV lift generation as well as the equation of motion for its translatory motion will be derived and elaborated.

Some results from the authors' previous analysis [31–34] provide the establishment of Coandă MAV spherical configuration baseline. The equations derived for the baseline configuration are significant for establishing preliminary design configuration concepts, and can be readily modified for other configurations for assessment, comparative and improvement purposes. CFD visualization studies will be instrumental in gaining in-depth understanding of the analytical and physical model development for further analysis.

Based on the physical and mathematical model conceived, some basic results were obtained to describe the physics of the flow field associated with the Coandă effect jet sheets. Having developed the basic fluid-dynamic analysis of the Coandă MAV lift generation, the equation of motion for Coandă MAV in translatory motion can be derived.

Various CFD studies have also indicated that there are still significant discrepancies between CFD and experimental studies [5, 15], which necessitate the existence of specific baseline configurations for validation purposes. Coandă MAV is expected to be capable of maneuvering as illustrated in **Figure 1 (a)** and **(b)**, and the analysis carried out here is associated with hovering condition, which should give further perception into its hovering performance.

The analysis carried out here is associated with hovering and cruising conditions, which should give further awareness on and can be further elaborated into Coandă MAV maneuvering performance. The baseline analysis on Coandă MAV spherical configuration carried out here refers to and confirms the authors' previous analysis [31–35].

The generic and baseline physical and mathematical model developed have been utilized to obtain some basic results that are essential in describing the flow field and the physical phenomena related to the relevant surfaces influenced by the Coandă effect jet sheets. Comparison of the numerical computation results for some baseline cases with experimental data under similar conditions will be essential, while computational parametric study will be

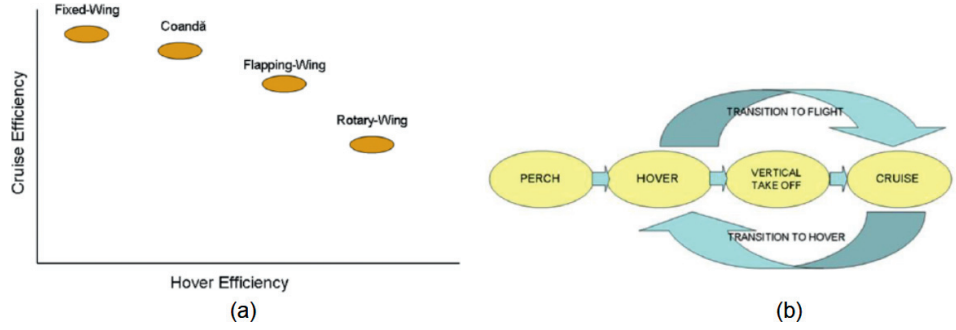

Figure 1. (a) An impression of the possible Coandă MAV qualitative performance in comparison to other flight vehicles (adapted from [10]), (b) Flight manoeuvring structure (adapted from [26]).

helpful as a preliminary effort for design and performance optimization. Some examples of Coandă effect applications and developments are illustrated in **Figure 2**.

It is with such objectives in mind that parametric studies may offer some clues on relevant parameters which may be utilized in a multivariable optimization (and to a larger scale, multidisciplinary optimization). The introduction of Coandă jet on both airfoils and aerodynamic surfaces results in enhanced L/D, which depends on the jet velocity or momentum coefficient. TE (Trailing-edge) rounding-off of in the introduction of the Coandă jet has been shown to be effective in increasing airfoil, L/D, as exemplified by recent applications of Coandă jet for STOL (Short Take-Off and Landing) or ESTOL (Extreme Short Take-Off and

	Some Coandă Effect Development and Applications		Examples/ Remarks
1	Some Coandă Inventions	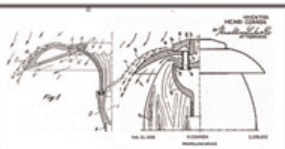	
2	Willard Custer, Englar and Campbell, Coandă-Effect Aircraft		Custer Channel Wing Aircraft; Lift due to " the speed of air, not the airspeed"
3	John Carver Meadow Frost Coandă-Effect Aircraft		Avrocar
4	Enhanced Lift by Coandă-Effect Circulation Enhancement		Antonov An-72
5			Boeing YC-14
6	Co-Flow Jet		US Navy Coandă-Effect Aircraft
7	California Polytechnique Group (Marshall, de la Montanya, etc)		Combined Blowing Circulation Control Application yo Extreme Short Take-Off & Landing
8	Automotive Application		Increase of base pressure, Coandă-Effect through exhaust gas for better traction

Figure 2. Some examples of Coandă effect applications and development (adapted from [14]).

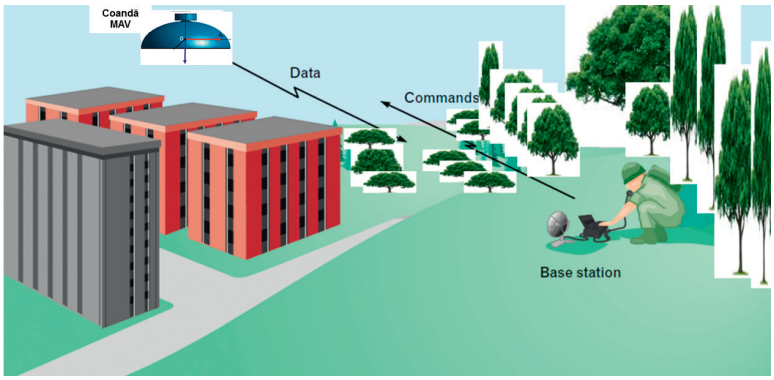

Figure 3. Micro-air-vehicle (MAV) used for reconnaissance. The MAV and a portable base station could remotely monitor the MAV under hostile conditions. Sensor data could be transferred in real time or stored on board the MAV (adapted from [37]).

Landing), e.g., S809. The study on Coandă jet application to wind turbines that could produce maximum total energy output of Coandă configured airfoil exceeding that predicted by Betz limit could provide further insight on Coandă jet application for MAV.

The test and evaluation of unmanned systems presents special challenges, but these challenges are amplified when one moves into the realm of micro-air-vehicles. Further complications arise when these MAVs are fully autonomous [37]. Autonomous MAVs must be able to sense the environment and guide their movement through it. To find their targets, autonomous MAVs should be able to identify them using object recognition procedure, and move toward their goal based on a path planning algorithm. The associated sensors can be employed for an aerial robotic MAV. MAVs have been utilized for surveillance that uses a data link and line-of-sight control, as illustrated in **Figure 3** (adapted from Davis et al. [37]); advanced MAVs can hover and navigate independently and carry multiple sensors. In addition, the production in large quantities of MAVs at low unit cost can be facilitated by exploiting microfabrication technology.

2. Coandă MAV Aerodynamics of hovering semi-spherical Coandă MAV as a baseline configuration

The Coandă MAV mathematical model utilized here follows closely that of Djojodihardjo et al. [31, 32] and Ahmed et al [33, 34]. The model was conceived to be generic and basic, and allow the application of first principles. The detail is summarized and reproduced here as a baseline reference for developments that may follow. In the Coandă MAV configuration illustrated in **Figure 4**, an actuator rotor is located at the center of the upper part of the body. As a baseline, the dimension of the rotor can be designed to be small as required. As illustrated in the figure, the flow being drawn by the actuator is entirely utilized for lift, by producing radial flow on the surface of the body as a Coandă jet blanket. In addition, like in a helicopter, a part of the flow produced by the actuator can pass through a vertical stream tube to produce lift (or thrust).

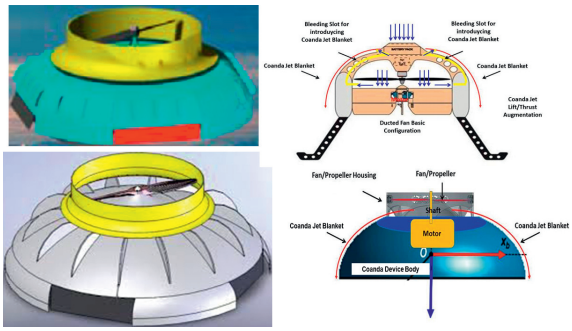

Figure 4. Various semi-spherical Coandă Devices utilizing a propeller to develop Coandă jet over its upper surface.

In the analysis of Coandă effect, momentum conservation principle in the sense of Euler equation is applied in the analysis to find the relevant aerodynamic forces and to define the performance parameters of the Coandă MAV. This procedure, applied for a baseline and simplified semi-spherical Coandă MAV configuration, is shown in **Figure 5**.

A rigorous analysis is then carried out to see how Coandă effect contributes to the Coandă MAV lift generation capability. For this purpose, the fundamental conservation analysis is applied on the control volume CV (dashed rectangle in **Figure 5**).

Applying the continuity equation (that is the mass conservation equation) given by $\dot{m}_{J.in} = \dot{m}_{J.out} = \dot{m}$, and assuming incompressible flow throughout, on the control volume enclosing the Coandă Blanket as depicted in **Figure 6**, there is obtained

$$\rho \cdot V_{j\text{-}R} \cdot 2\pi Rh = \rho \cdot V_{j\text{-}in} \cdot 2\pi R_i h_i = \rho \cdot V_{j\text{-}out} \cdot 2\pi R_o h_o \tag{1}$$

and

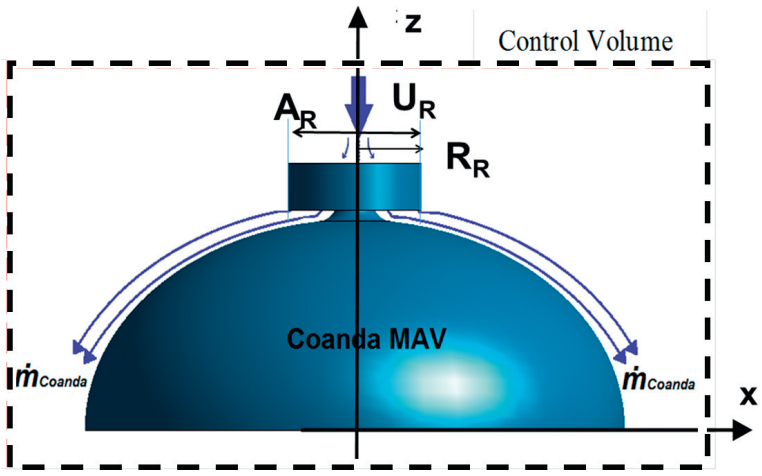

Figure 5. An equivalent semi-spherical Coandă MAV for Generic Analysis.

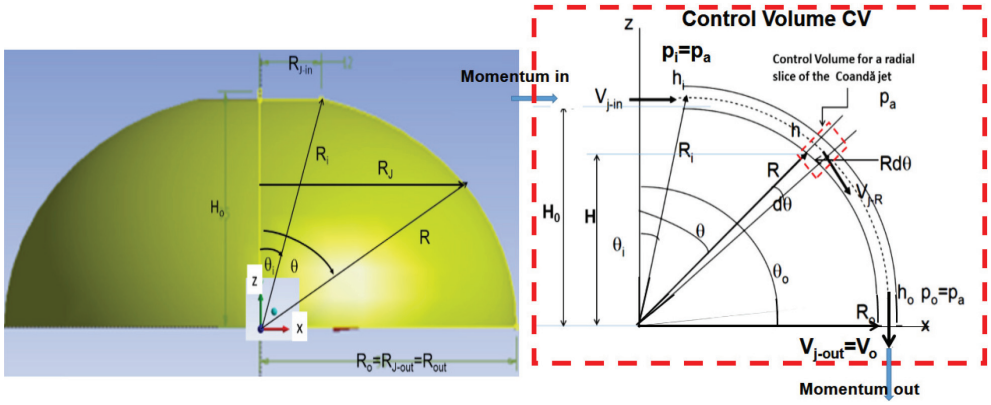

Figure 6. Schematic of Coandă jet blanket for a spherical MAV momentum balance.

$$V_{j\text{-}R} = \frac{R_i h_i}{R h_R} V_{j\text{-}in} = \frac{\dot{m}}{2\pi\rho R h_R}$$
$$V_{j\text{-}out} = \frac{R_i h_i}{R_o h_o} V_{j\text{-}in} = \frac{\dot{m}}{2\pi\rho R_o h_o} \quad (2)$$

where $V_{j\text{-}R}$ is the jet flow velocity, R is the vehicle body radius, h is the jet slot thickness and $\dot{m}$ is the jet mass flow rate. $V_{J\text{-}out}$, R_o, h_o, $V_{J\text{-}in}$ R_i, and h_i refer to velocity, radius and jet thickness at the outlet and inlet, respectively, of the Coandă jet blanket. As depicted in **Figure 6**, the, the Coandă jet blanket is exposed to the ambient pressure pa, which is then the prevailing static pressure on it. The momentum equation applied to the control volume in the z (vertical) direction can be differentiated into the contribution due to the Coandă Blanket momentum and the pressure difference on the body due to Coandă Blanket:

$$\begin{pmatrix}\text{Total Lift force}\\ \text{due to Coandă Blanket}\end{pmatrix} = \begin{pmatrix}\text{Vertical component of momentum}\\ \text{flux balance due to Coandă Blanket}\end{pmatrix} + \begin{pmatrix}\text{Pressure difference on the body}\\ \text{of MAVsubject to Coandă Blanket}\end{pmatrix} \quad (3)$$

The contribution of lift from the momentum flux through the control volume CV in the y (vertical) direction is given by

$$\begin{pmatrix}\text{Force on the } \textit{Coandă MAV}\\ \text{in the z-direction}\end{pmatrix} = \begin{pmatrix}\text{Rate of Momentum In}\\ \text{into CV the y-direction}\end{pmatrix} - \begin{pmatrix}\text{Rate of Momentum Out}\\ \text{of CV in the z-direction}\end{pmatrix} \quad (4)$$

with z and force positive in the upward direction.

It is noted that the momentum in the radial direction does not contribute to lift. Therefore, as exhibited in **Figure 6**, the momentum equation in the y direction for the control volume CV is

$$F_{Coanda\,jet\,Blanket} = \dot{m}\, V_{J\text{-}out} = 2\pi R_i h_i \rho \cdot V_{J\text{-}in} \cdot V_{J\text{-}out} \tag{5}$$

Before proceeding to analyze the contribution of the forces on the Coandă MAV due to the pressure difference across the control volume, the energy equation applied to the control volume will be considered. It reads

Energy input to the control volume = Energy output from the control volume

In the control volume analysis throughout this work, uniform properties across the sectional areas at the input and output of the Coandă jet blanket have been assumed. The entrainment energy exchange between the ambient air and the Coandă jet blanket as well as other energy losses have been ignored.

Hence, referring again to **Figure 6**, taking into consideration the mass conservation and assuming similar ambient pressure at the inlet and outlet, the application of the energy conservation equation within the control volume which only involves the fluid flow along the Coandă jet blanket results in

$$\begin{aligned} \frac{1}{2} m_{in} {V_{J-in}}^2 &= \frac{1}{2} m_{out} {V_{J-out}}^2 \quad [M]\left[L^2T^{-2}\right] = \left[MLT^{-2}\right][L] \\ 2\pi\rho V_{J-in} h_{J-in} R_{in} V_{J-in} &= 2\pi\rho V_{J-out} h_{J-out} R_{out} V_{J-out} = 2\pi\rho V_J h_J R_J V_J \\ \dot{m}_{in} V_{J-in} &= \dot{m}_{out} V_{J-out} = \dot{m}_J {V_J}^2 \\ V_{J-in} &= V_{J-out} = {V_J}^2 \end{aligned} \tag{6}$$

Therefore, upon substitution of Eq. (6) into Eq. (5), one obtains

$$L_{\substack{Momentum \\ Coanda\,jet\,blanket}} = F_{Coanda\,jet\,Blanket} = \dot{m}\, V_{j\text{-}out} = 2\pi R_i h_i \rho \cdot {V_{J\text{-}in}}^2 \tag{7}$$

Using the model as shown in **Figure 7**, the underbody represented by the outer part of the lower surface of the control volume as well as the wake of the MAV are at ambient pressure. The entire flow entering the rotor represented by the actuator disk can be utilized for the Coandă jet blanket after leaving the actuator disk with velocity $V_{J\text{-}in}$, and then leaves the Coandă MAV after being ejected as $V_{J\text{-}out}$ and combined with the entrained fluid outside the Coandă jet blanket as the wake. If part of the flow is used to feed the Coandă jet blanket, then the rest of the flow leaving the actuator will form a stream tube leaving the Coandă MAV like a ducted fan and eventually will be combined with the exiting jet from the Coandă jet blanket.

Noting the specific characteristics of Coandă effect is attributed to the attachment of a jet to a curves surface, an analysis will be performed on the Coandă device control volume depicted in **Figure 6** by focusing on a control volume enclosing radial slice of the Coandă blanket with thickness h at (R, θ). Considering a balance of force along the radial direction R in the Coandă jet slice control volume, centrifugal effects along R allows a radial pressure gradient to prevail perpendicular to Coandă jet; hence

http://dx.doi.org/10.5772/intechopen.70157

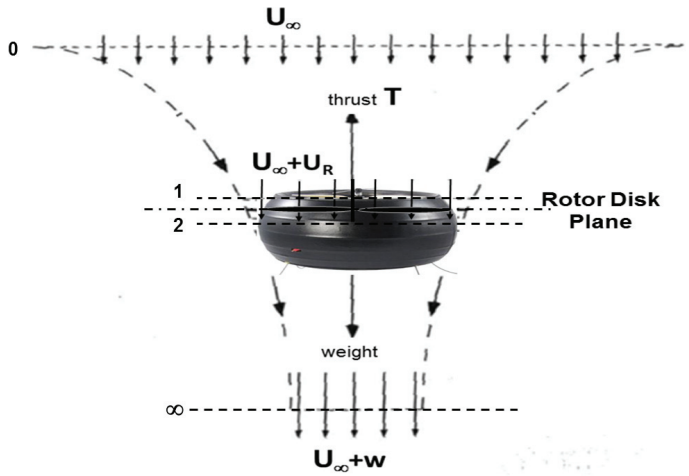

Figure 7. Control volume analysis of Coandă MAV actuator disk schematic.

$$\left(p_a - p_{\substack{J-\theta \\ Coandă-Surface}}\right) R_{J-\theta} d\theta = radial\text{-}acceleration \cdot \rho h_{J-\theta} R_{J-\theta} d\theta \tag{8a}$$

where

$$radial\text{-}acceleration = \frac{V_{J-\theta}{}^2}{R_{J-\theta}} \tag{8b}$$

so that

$$p_{\substack{J-\theta \\ Coandă\text{-}Surface}} = p_a - \frac{V_{J-\theta}{}^2}{R_{J-\theta}} \cdot \rho h_{J-\theta} \quad \left[\frac{MLT^{-2}}{L^2}\right] - \left[\frac{L^2T^{-2}}{L}\right]\left[\frac{ML}{L^3}\right] \tag{8c}$$

Here the ambient pressure p_a acts on the outer surface of the Coandă jet blanket, while $p_{J\text{-}\theta}$ acts on the lower surface of the Coandă jet blanket, thus on the upper surface of the Coandă MAV.

The contribution of the vertical forces on the Coandă MAV due to the pressure difference across the control volume can now be considered. This is then give by

$$L_{pressure} = Pressure\ Force_{CV-upper} - Pressure\ Force_{CV-lower} = 2\pi \int_{R_{J-\theta}\ at\ jat\ inlet}^{R_{J-\theta}=R_{J-out}} p_{J-\theta} R_{J-\theta} dR_{J-\theta} - p_a \pi R_{J-\theta}{}^2 \tag{9a}$$

Substituting Eq. (8c), the vertical force due to pressure difference is then given by

$$L_{pressure} = Force_{\substack{Pressure \\ CV-upper}} - Force_{\substack{Pressure \\ CV-lower}} = 2\pi \int_{R_{J-\theta}\ at\ jat\ inlet}^{R_{J-\theta}=R_{J-out}} \left(-\frac{{V_{J-\theta}}^2}{R_{J-\theta}} \cdot \rho h_{J-\theta}\right) R_{J-\theta} dR_{J-\theta} \tag{9b}$$

Since either the plenum chamber between the upper curved surface or the bottom part of the Coandă MAV is at the atmospheric pressure p_a, then p_a in Eq. (9b) will drop off. Hence

$$\begin{aligned} L_{pressure} = Force_{\substack{Pressure \\ CV-upper}} - Force_{\substack{Pressure \\ CV-lower}} &= 2\pi \int_{R_{J-\theta}\ at\ jat\ inlet}^{R_{J-\theta}=R_{J-out}} \left(-\frac{{V_{J-\theta}}^2}{R_{J-\theta}} \cdot \rho h_{J-\theta}\right) R_{J-\theta} dR_{J-\theta} \\ &= -2\pi \int_{R_{J-in}}^{R_{J-out}} {V_{J-\theta}}^2 \cdot \rho h_{J-\theta} dR_J \end{aligned} \tag{10a}$$

which is a downward force, or an upward force

$$L_{pressure} = Force_{\substack{Pressure \\ CV-lower}} - Force_{\substack{Pressure \\ CV-upper}} = 2\pi \int_{R_{J-in}}^{R_{J-out}} {V_{J-\theta}}^2 \cdot \rho h_{J-\theta} dR_J \tag{10b}$$

$$L_{pressure} = 2\pi \int_{R_{J-in}}^{R_{J-out}} {V_{J-\theta}}^2 \cdot \rho h_{J-\theta} dR_J = \dot{m} \int_{R_{J-in}}^{R_{J-out}} \frac{V_{J-\theta}}{R_J} dR_J = \dot{m} V_{J-in} \left(\ln R_{J-out} - \ln R_{J-in}\right) \tag{10c}$$

Hence, the total lift due to Coandă jet blanket momentum and Coandă jet blanket pressure difference, or the total lift force due to the rate of momentum in the vertical direction and due to pressure difference across the control volume becomes

$$L_{Coanda\ MAV} = L_{\substack{Momentum \\ Coanda\ jet\ blanket}} + L_{pressure} = 2\pi R_o h_o \rho_J \cdot V_{J.in}^2 + \dot{m} V_{J-in} \ln \frac{R_{J-out}}{R_{J-in}} \tag{11a}$$

or

$$L_{Coanda\ MAV} = \dot{m} V_{J-in} \left(1 + \ln \frac{R_{J-out}}{R_{J-in}}\right) \tag{11b}$$

Defining Coandă jet input momentum rate as

$$2\pi R_{in} h_{J-in} \rho_J {V_{J.in}}^2 = \dot{m}_{J.in} V_{J.in} \tag{12}$$

The Coandă jet momentum coefficient (as initially defined by Poisson-Quinton [38]) is conventionally defined as

$$C_\mu = \frac{\dot{m}_{J.in} V_{J.in}}{\frac{1}{2}\rho U^2 S} = \frac{2\pi R_{in} h_{in} \rho_J {V_{J.in}}^2}{\frac{1}{2}\rho U^2 S} \tag{13}$$

where U and S should be referred to the ambient reference condition, which here can be chosen to be either the free stream velocity U_∞ and the lifting area of the Coandă device (MAV), πR_o^2, respectively, or the downward inlet velocity to the Coandă MAV jet inducing rotor, i.e., the velocity of the incoming downward flow to the rotor U_R (see **Figure 5**) and the area of the rotor A_R. Hence,

$$C_{\mu-FS} = \frac{\dot{m}_{J.in} V_{J.in}}{\frac{1}{2}\rho U_\infty{}^2 \pi R_{out}{}^2} \tag{14a}$$

or

$$C_{\mu-Rotor} = \frac{\dot{m}_{J.in} V_{J.in}}{\frac{1}{2}\rho U_R{}^2 \pi R_R{}^2} \tag{14b}$$

For rotor in-flow completely dedicated for Coandă jet, from conservation of mass principle

$$\dot{m}_{J.in} = \rho U_R \pi R_R{}^2 \tag{15}$$

and

$$C_{\mu-Rotor} = \frac{\dot{m}_{J.in} V_{J.in}}{\frac{1}{2}\rho U_R{}^2 \pi R_R{}^2} = \frac{2\pi R_{in} h_{in} \rho V_{J.in}{}^2}{\frac{1}{2}\rho U_R{}^2 \pi R_R{}^2} = 4\frac{R_{in} h_{in}}{R_R{}^2}\frac{V_{J.in}{}^2}{U_R{}^2} \tag{16}$$

Hence,

$$C_{\mu-Rotor} = \frac{2\pi R_{J-in} h_{J-in} \rho V_{J.in}{}^2}{\frac{1}{2}\pi R_R{}^2 \rho U_R{}^2} = 4\left(\frac{h_{J-in}}{R_{J-in}}\right)\left(\frac{V_{J.in}}{U_R}\right)^2 \equiv 4\left(\frac{h_{J-in}}{R_R}\right)\left(\frac{V_{J.in}}{U_R}\right)^2 \tag{17}$$

For convenience, in line with the rationale elaborated in [31–34], an indicator of the effectiveness of the Coandă jet device (MAV) to produce lift from rotor-like momentum rate input from the ambient air, a Performance Measure PM can be defined. Following the previous development and different from [31–34], a new Performance Measure P_M can be defined as

$$P_{M-Coandă} = \frac{Lift}{Rate\ of\ Momentum\ Input_{Coandă}} = \frac{\dot{m} V_{J-in}\left(1 + \ln\frac{R_{J-out}}{R_{J-in}}\right)}{2\pi R_{in} h_{in} \rho_J V_{J.in}{}^2} = \left(1 + \ln\frac{R_{J-out}}{R_{J-in}}\right) \tag{18}$$

Utilizing Eq. (16) and assuming $R_{J\text{-}in} \approx R_R$ (without loss of generalities), $C_{\mu\text{-Rotor}}$ can be expressed as

$$C_{\mu-Rotor} = 4\frac{R_{in} h_{in}}{R_R{}^2}\frac{V_{J.in}{}^2}{U_R{}^2} \approx 4\frac{h_{J-in}}{R_{J-in}}\frac{V_{J.in}{}^2}{U_R{}^2} \approx 4\frac{h_{J-in}}{R_R{}^2}\frac{V_{J.in}{}^2}{U_R{}^2} \tag{19}$$

The performance measure (PM) can alternatively be written in terms of momentum coefficient as

$$P_{M-Coandă} = \frac{Lift}{Rate\ of\ Momentum\ Input_{Coandă}} = \frac{\dot{m}V_{J-in}\left(1+\ln\frac{R_{J-out}}{R_{J-in}}\right)}{2\pi R_{J-in}h_{J-in}\rho_J {V_{J.in}}^2} = 4\frac{R_{J-in}h_{J-in}}{{R_R}^2}\frac{{V_{J.in}}^2}{{U_R}^2}\frac{\left(1+\ln\frac{R_{J-out}}{R_{J-in}}\right)}{C_{\mu-Rotor}} \tag{20a}$$

or

$$P_{M-Coandă} = \frac{Lift}{Rate\ of\ Momentum\ Input_{Coandă}} = \frac{\dot{m}V_{J-in}\left(1+\ln\frac{R_{J-out}}{R_{J-in}}\right)}{2\pi R_{J-in}h_{J-in}\rho_J {V_{J.in}}^2} \approx 4\frac{h_{J-in}}{R_{J-in}}\frac{{V_{J.in}}^2}{{U_R}^2}\frac{\left(1+\ln\frac{R_{J-out}}{R_{J-in}}\right)}{C_{\mu-Rotor}} \tag{20b}$$

The above derivation is carried out on a Coandă MAV configuration with actuator (rotor) dedicated to produce Coandă Jet Blanket. It has tacitly been assumed that the Coandă MAV jet blanket covers the entire upper surface of the Coandă MAV ("perfect blanket"). Therefore, for this Coandă MAV semi-spherical configuration design, which may represent a baseline of other similar Coandă MAV with moderately different upper surface curvature with MAV with ("perfect blanket"), the wake of the Coandă MAV is shed as a wake following the body of the Coandă MAV. Such situation can be verified at a later stage using CFD simulation for closely modelled flow situation. Then it will be reasonable to assume that the static pressure of the wake of the Coandă MAV the ambient pressure p_a prevails. For Coandă MAV with ducted-fan-line configuration, an actuator disk model should be added in the force system in addition to those elaborated above.

3. Lift generated by the rotor (actuator disk)

Figure7 depicts a MAV configuration consisting of a propeller at the center of the upper part with radially bled flow to generate Coandă effect along the upper surface of the spherical MAV. Here, UR is the axial inlet flow through the actuator along the vertical actuator shaft direction.

Therefore, the lift generated by the propeller can be calculated using actuator disk theory [39–42]

$$Lift_{actuator} = 2\pi\rho {R_R}^2 {U_R}^2 \tag{21}$$

which should be added to Eq. (12), and modified to account for the actuator disk cylindrical part with assumed uniform radius R_I. Therefore, the lift of the Coandă MAV due to the actuator and Coandă blanket becomes

$$Lift_{\substack{Spherical-Coanda\ MAV \\ with-actuator}} = Lift_{\substack{Spherical-Coanda\ MAV \\ without-actuator}} + Lift_{actuator} = \dot{m}V_{J-in}\left(1+\ln\frac{R_{J-out}}{R_{J-in}}\right) + 2\pi\rho {R_R}^2 {U_{R\text{-}actuator}}^2$$
$$= \dot{m}V_{J-in}\left(1+\ln\frac{R_{J-out}}{R_{J-in}}\right) + 2\dot{m}_R U_{R\text{-}actuator} \tag{22}$$

Here, the mass flow rate into the actuator disk is given by

$$\dot{m}_R \equiv \pi\rho {R_R}^2 U_{R\text{-}actuator} \tag{23}$$

and one may assume that

$$U_\infty \approx 0 \tag{24}$$

and from actuator disk theory [40–43]

$$w = 2U_{R\text{-}actuator} \tag{25}$$

In this elaboration, the Betz limit [43], which is the theoretical maximum efficiency of the actuator disk ($\eta = 16/27 \approx 59.26\%$), is not considered.

A remark is in order here associated with the Coandă MAV as illustrated in **Figures. 4**, and **5** as represented and the top of **Figure 7** above. To avoid the MAV body counter-rotates due to the rotor, counter-rotating rotors can be utilized as the actuator. Eqs (13)–(15) remain valid as the baseline equation, but the design configuration in the conceptual and detailed design of the Coandă MAV should be elaborated accordingly.

Several alternatives can be considered for the Coandă MAV with actuator configuration. First, if all the flow into the actuator is utilized for the Coandă MAV, one may obtain a comparison between the lift produced by Coandă MAV without actuator and ducted fan which utilizes actuator flow only. Hence

$$\frac{Lift_{\substack{Spherical-Coanda\ MAV \\ without-actuator}}}{Lift_{actuator}} = \frac{\dot{m}V_{J-in}\left(1+\ln\frac{R_{J-out}}{R_{J-in}}\right)}{2\pi\rho {R_R}^2 {U_R}^2} == \frac{1}{2}\left(\frac{\dot{m}}{\dot{m}_{actuator}}\right)\left(1+\ln\frac{R_{J-out}}{R_{J-in}}\right)\frac{V_{J-in}}{U_{R\text{-}actuator}}$$
$$= \frac{\Phi_{Coandă-mass}}{2}\left(1+\ln\frac{R_{J-out}}{R_{J-in}}\right)\frac{V_{J-in}}{U_{R\text{-}actuator}} \tag{26}$$

Here, the ratio between the mass flow rates injected for Coandă MAV jet $\dot{m}_J$ and the mass flow rate entering the rotor $\dot{m}_R$ is defined as the Coandă MAV mass ratio $\Phi_{\text{Coandă-mass}}$.

$$\Phi_{Coandă-mass} = \frac{\dot{m}_J}{\dot{m}_R} \tag{27}$$

Eq. (26) establishes the benefit of Coandă MAV jet blanket lift compared to actuator (ducted fan, or helicopter) lift,

Eq. (22) can be written as

$$Lift_{\substack{Spherical-Coanda\ MAV\\ with-actuator}} = \dot{m}_J V_{J-in}\left(1+\ln\frac{R_{J-out}}{R_{J-in}}\right)+2\pi\rho {R_R}^2 {U_{R\text{-}actuator}}^2 = \dot{m}_J V_{J-in}\left(1+\ln\frac{R_{J-out}}{R_{J-in}}\right)+2\dot{m}_R U_{R\text{-}actuator}$$
$$= \dot{m}_R U_{R\text{-}actuator}\left\{\Phi_{Coand\check{a}-mass}\frac{V_{J-in}}{U_{R\text{-}actuator}}\left(1+\ln\frac{R_{J-out}}{R_{J-in}}\right)+2\right\} \tag{28}$$

Then the performance measure (PM) for Lift can alternatively be written in terms of Coandă MAV mass ratio $\Phi_{Coanda-mass}$ as

$$P_{M-Lift} \equiv \frac{Lift_{\substack{Spherical-Coanda\ MAV\\ with-actuator}}}{\dot{m}_R U_{R\text{-}actuator}} = \left\{\Phi_{Coanda-mass}\frac{V_{J-in}}{U_{R\text{-}actuator}}\left(1+\ln\frac{R_{J-out}}{R_{J-in}}\right)+2\right\} \tag{29}$$

If all the actuator flow is utilized for the Coandă MAV jet blanket, Eq. (28) reduces to

$$Lift_{\substack{Spherical-Coanda\ MAV\\ with-actuator}} = \dot{m}_R\left\{V_{J-in}\left(1+\ln\frac{R_{J-out}}{R_{J-in}}\right)\right\} \tag{30}$$

and the performance measure (PM) for Lift of Coandă MAV Eq. (29) reduces to

$$P_{M-Lift} \equiv \frac{Lift_{\substack{Spherical-Coanda\ MAV\\ with-actuator}}}{\dot{m}_R U_{R\text{-}actuator}} = \left\{\frac{V_{J-in}}{U_{R\text{-}actuator}}\left(1+\ln\frac{R_{J-out}}{R_{J-in}}\right)+2\right\} \approx \left\{\frac{R_{J-in}}{2h_{J-in}}\left(1+\ln\frac{R_{J-out}}{R_{J-in}}\right)+2\right\} \tag{31}$$

4. Flight dynamic analysis for semi-spherical Coandă MAV in translatory motion

4.1. System of coordinates

For setting the equation of motion of the Coandă MAV, the system coordinates that are required will be defined. Four main reference frames can be identified for this purpose; these are the inertial coordinate system, the local horizon reference frame, the body reference frame, and the wind reference frame. These reference frames are shown in **Figure 8**.

For simplicity and instructiveness, only two-dimensional coordinate systems in the plane of symmetry of the Coandă MAV will be defined. These four frame of reference are:

1. **Inertial coordinate system**, which is used for defining and the application of the Newton's law of motion. In two dimensions, this coordinate system is depicted by the $O_E$xyz.
2. **The local horizon coordinate system $Ox_hy_hz_h$,** which is fixed at the center of mass of the vehicle, and is parallel with the earth Inertial Coordinate system.
3. **The body coordinate system $Ox_by_bz_b$,** which is fixed to the vehicle and follows a conveniently chosen axis of the vehicle.

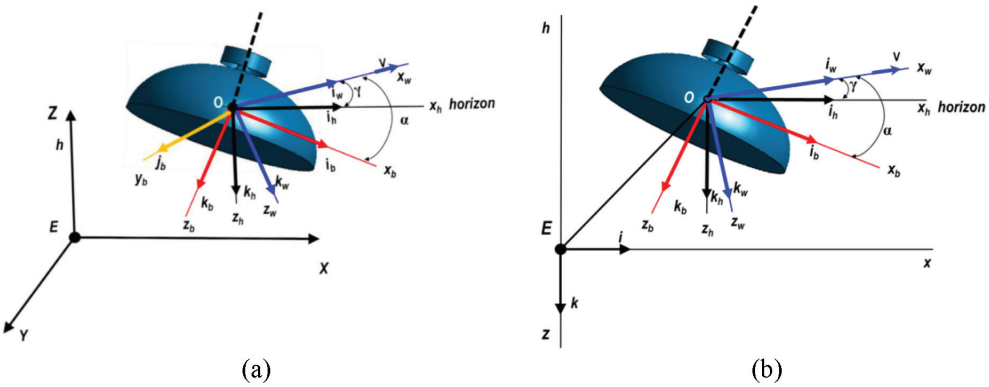

Figure 8. (a) The details of the four coordinate systems for Coandă MAV flight vehicle; (b) Axes systems in the vertical plane perpendicular to the Earth's Surface.

4. **The wind axes system $Ox_wy_wz_w$** which moves with the vehicle and the x_w axis coincides with the flight path of the vehicle, hence its velocity vector.

The wind axes are oriented to the flight path angle γ relative the local horizon axes, as shown in **Figure 8a**, and by the angle of attack α relative to the body axes. **Figure 8b** exhibits the two dimensional configuration in the vertical plane perpendicular to the earth surface.

4.2. Flight dynamic analysis

Without loss of generalities, the equation of motion of the flight dynamics of Coandă MAV in translatory motion is developed in the vertical plane perpendicular to the earth motion (two-dimensional planar motion). The hovering state, illustrated in **Figure 9**, is employed as a reference. In addition, in the present analysis, only the Coandă MAV jet is incorporated in the

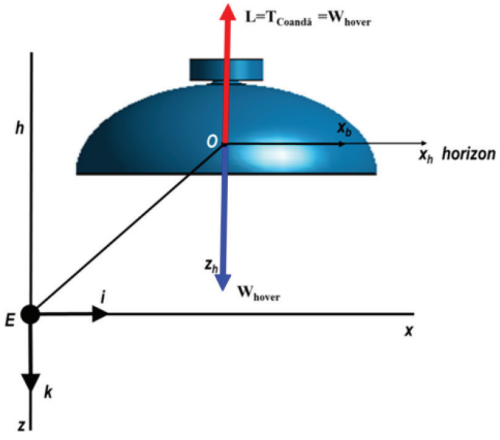

Figure 9. Coordinate systems for Coandă MAV in hover, in two-dimensional flight (at the vertical plane of symmetry of the Coandă MAV).

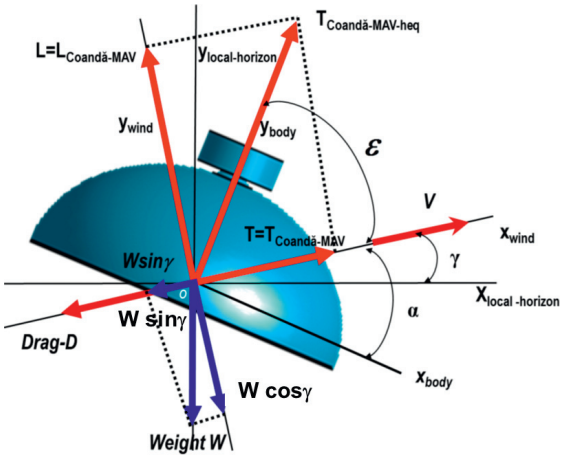

Figure 10. Coandă MAV schematic in two-dimensional translatory motion in the vertical plane (at the vertical plane of symmetry and motion).

derivation. The influence of the actuator can be linearly superposed as demonstrated in the hover case, Eqs. (13)–(15).

Balance of forces in the free-body diagram exhibited in **Figure 10** implies

$$L_{Hover} \equiv T_{Coandă-MAV} = W_{Coandă-MAV-Take-off} \tag{32}$$

The use of the mass conservation equation

$$\dot{m}_{J-in} = 2\pi\rho R_{J-in} h_{J-in} V_{J\text{-}in} \tag{33}$$

and the use of the Coandă lift from Eq. (11b) then leads to:

$$L_{Hover} \equiv T_{Coandă-MAV} = 2\pi\rho R_{J-in} h_{J-in} V_{J\text{-}in}^2 \left(1 + \ln\frac{R_{J-out}}{R_{J-in}}\right) = W_{Coandă-MAV-Take-off} \tag{34}$$

Further, simplifying assumptions will be made for the development of the equation of motion during translatory motion. This equation could be further refined to incorporate more realistic cases.

These comprise

1. During hover, the thrust of the Coandă MAV will not be influenced by the inclination of the Coandă MAV. This assumption can be later modified for more elaborate analytical model, which could be assisted by CFD simulation.

2. The thrust generated by the Coandă MAV during translatory motion is assumed to stay the same; therefore:

$$\begin{aligned} T_{Coandă-MAV} &= \dot{m}_{J-in} V_{J-in} \left(1 + \ln \frac{R_{J-out}}{R_{J-in}}\right)|_{hover-equivalent} \\ &= 2\pi\rho R_{J-in} h_{J-in} V_{J\text{-}in}^2 \left(1 + \ln \frac{R_{J-out}}{R_{J-in}}\right)|_{hover-equivalent} \end{aligned} \tag{35}$$

Using the basic flight dynamic equation for flight vehicle, the equation of motion of the Coandă MAV in translational motion in the two-dimensional vertical plane can be written by referring to **Figure 10**

Kinematic:

$$\dot{x} = V\cos\gamma \quad \left[LT^{-1}\right] \tag{36}$$

$$\dot{h} \equiv \dot{y} = V\sin\gamma \quad \left[LT^{-1}\right] \tag{37}$$

$$\varepsilon = \tan^{-1}\frac{\ddot{y}_{wind}}{\dot{V}} = \tan^{-1}\frac{g(L - W\cos\gamma)}{W\dot{V}} = \tan^{-1}\frac{g}{\dot{V}}\frac{(L - W\cos\gamma)}{W} \quad [-] \tag{38}$$

$$\dot{\varepsilon} = \tan^{-1}\frac{\ddot{y}_{wind}}{V} = \tan^{-1}\frac{g(L - Wcos\gamma)}{WV} = \tan^{-1}\frac{g}{V}\frac{(L - W\cos\gamma)}{W} \quad \left[T^{-1}\right] \tag{39}$$

Coandă MAV Fluid Dynamics:

$$T_{Coandă-MAV} = 2\pi\rho R_{J-in} h_{J-in} V_{J\text{-}in}^2 \left(1 + \ln \frac{R_{J-out}}{R_{J-in}}\right) \quad \left[MLT^{-2}\right] \tag{40}$$

Coandă MAV Flight Dynamics:

$$\dot{V} = (g/W)\left(T_{Coandă\ MAV-heq} cos\varepsilon - D - W\sin\gamma\right) \quad \left[LT^{-2}\right] \tag{41}$$

$$\ddot{y} = (g/W)\left(T_{Coandă\ MAV-heq}\sin(\varepsilon + \gamma) - W - D\sin\gamma\right) \quad \left[LT^{-2}\right] \tag{42}$$

Weight-Fuel Consumption:

$$\dot{W} = -CT \quad \left[MT^{-1}\right] \tag{43}$$

where C is the specific fuel consumption, weight per unit thrust [Newton/Newton].

The above relationships are derived for balance of forces and Newton's equation for semi-spherical Coandă MAV, which is treated as a point mass moving in a plane perpendicular to the planar Earth.

5. Performance measure

5.1. Performance measure during hover

The feasibility of using Coandă techniques to enhance aerodynamic performance of Coandă MAV can be outlined through some non-dimensional quantities of performance measure. The most logical measure that has commonly been utilized is the Coandă jet momentum coefficient, C_μ(Poisson-Quinton [38]), which are defined as (14a) or (14b), as appropriate:

$$C_{\mu-\text{Coandă}-jet} = \frac{\dot{m} V_{\text{Coandă}-jet}}{\frac{1}{2}\rho_j V_\infty^2 A_{ref}} \tag{44a}$$

or

$$C_{\mu-\text{Coandă}-jet} = \left[\frac{\dot{m}_{J.in} V_{J.in}}{\frac{1}{2}\rho {U_\infty}^2 \pi {R_{out}}^2}\right]_{\text{Coandă}-jet} \tag{44b}$$

or

$$C_{\mu-\text{Coandă}-jet} = \left[\frac{\dot{m}_{J.in} V_{J.in}}{\frac{1}{2}\rho {U_\infty}^2 \pi {R_{out}}^2}\right]_{\text{Coandă}-jet} \tag{44c}$$

One can define another Performance Measure to evaluate the aerodynamic performance of spherical Coandă MAV considered here during hover and lift-off, by assessing the output lift as compared to the input momentum rate, following consideration discussed in [31, 33–34]. These are given by Eqs. (18) and (20) following a different derivation elaborated in previous section.

The Performance Measure may be defined in a different way by referring to the rate of the energy of the Coandă jet ejected at its ideal inlet velocity $V_{j\text{-}out}$ at its peripheral outlet, and comparing it to the rate of momentum influx of the Coandă jet times its inlet velocity $V_{j\text{-}in}$ (non-dimensional):

$$P_{\substack{M-E \\ \text{Spherical Coandă}-MAV}} = \frac{\textit{Lift produced by Coandă MAV} \text{ times } V_{J-out} \textit{ at its peripheral outlet}}{\textit{the rate of momentum influx of the Coandă jet times its inlet velocity } V_{J-in}}$$

$$= \frac{\dot{m} V_{J-in} V_{J-out}\left(1 + \ln\frac{R_{J-out}}{R_{J-in}}\right)}{2\pi R_{in} h_{in} \rho_J {V_{J.in}}^3} = \left(1 + \ln\frac{R_{J-out}}{R_{J-in}}\right)\frac{V_{J-out}}{V_{J.in}} \tag{45}$$

based on Coandă MAV geometry and kinematics, or

$$P_{\substack{M-E \\ \text{Spherical Coandă}-MAV}} = \frac{\textit{Lift produced by Coandă MAV} \text{ times } V_{J-out} \textit{ at its peripheral outlet}}{\textit{the rate of momentum influx of the Coandă jet times its inlet velocity } V_{J-in}}$$

$$\approx 4\frac{h_{J-in}}{R_{J-in}}\frac{{V_{J.in}}^2}{{U_R}^2}\frac{\left(1+\ln\frac{R_{J-out}}{R_{J-in}}\right)}{C_{\mu-Rotor}}\frac{V_{J-out}}{V_{J.in}} \tag{46}$$

based on Coandă MAV geometry, kinematics and momentum coefficient. Although Eq. (18) is based on rate of momentum flux while Eq. (45) on energy input, both equations are similar.

For the baseline semi-spherical Coandă MAV case considered, $V_{J\text{-}out}/V_{J\text{-}in}$ will be the same, and hence Eqs. (45) and (46) reduces to Eqs. (18) and (20). This notion may not be met in more general cases. Since the theoretical analysis does not consider viscosity and other losses, more information is required to insure uniqueness. Further realistic assumption can be drawn by carrying out computational fluid dynamic (CFD) simulation and visualization, which incorporate viscous effects and turbulence, to add further understanding into the problem and introduce further refinement in the theoretical modeling and analysis.

5.2. Performance measure during translation

For further reference and as a baseline, Performance Measure can be defined for two cases during translation: for level flight and for climbing.

For level flight (by referring to **Figure 11**):

$$\begin{aligned} P_{M\,\underset{LevelFlight}{\text{Coandă}-MAV}} &= \frac{Power\ required\ to\ overcome\ Drag}{Power\ Input\ by\ Coandă\ jet\ action} \\ &= \frac{Drag * Velocity}{Coandă\ Jet\ \text{Momentum Gain} * Coandă\ Jet\ \text{Velocity In}} \\ &= \frac{D\cdot V\cos\gamma^2}{\dot{m}{V_{j\text{-}in}}^2}\left[\frac{ML^2T^{-2}}{ML^2T^{-2}}\right] \end{aligned} \tag{47}$$

For purely level flight, $\gamma = 0$ (by referring to **Figures 10** and **11**). Taking into account that the prevailing cross-sectional area of the Coandă MAV perpendicular to the flow is depicted in **Figure 11(b)**, Eq. (47) reduces to:

$$P_{M\,\underset{LevelFlight}{\text{Coandă}-MAV}} \approx \frac{1}{4}C_{D\to x}\frac{\pi\rho{R_o}^2 sin\alpha}{\dot{m}_i}\frac{V^3}{{V_{j\text{-}in}}^2} \tag{48}$$

Alternatively, another related Performance Measure can be defined as follows:

$$P'_{M\,\underset{LevelFlight}{\text{Coandă}-MAV}} \equiv \frac{P_{M\,\underset{LevelFlight}{\text{Coandă}-MAV}}}{C_{D\to x}sin\alpha} \approx \frac{1}{4}\frac{\pi\rho{R_o}^2}{\dot{m}_i}\frac{V^3}{{V_{j\text{-}in}}^2} \tag{49}$$

Here $C_{D\to x}$ is the Drag coefficient of the Coandă MAV in the x direction, and α is its inclination angle with respect to the flight direction as depicted as depicted in **Figure 11**.

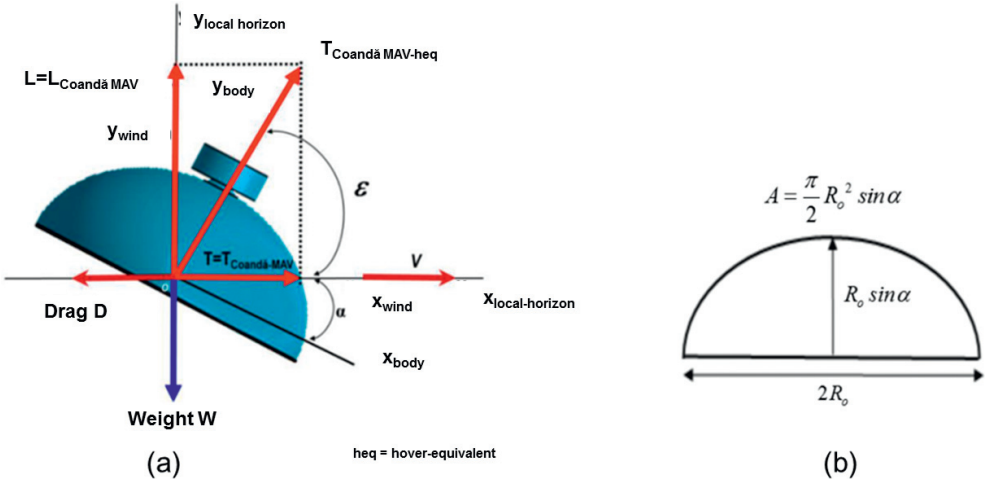

Figure 11. Schematic of Coandă MAV in two-dimensional cruising motion in the vertical plane of symmetry and motion. Inset: Cross-sectional area perpendicular to direction of motion.

The general expression for the Performance Measure for climbing is:

$$\begin{aligned} P_{M\ \substack{\text{Coandă}\\-MAV\\\text{Climbing}}} &= \frac{\textit{Power required to Climb}}{\textit{Power Input by Coandă jet action}} \\ &= \frac{T_{Coandă-MAV} \bullet \dot{y} - D \bullet \dot{y} - W \bullet \dot{y}}{\text{Coandă } \textit{Jet Rate of} \text{ Momentum Gain} * \text{Coandă } \textit{Jet} \text{ Velocity In}} \\ &= \left(\frac{T(t) - (D\sin\gamma + W)}{\dot{m} V_{J\text{-}in}}\right)\frac{V\sin\gamma}{V_{J\text{-}in}} \end{aligned} \tag{50}$$

Here, all variables are taken for the same flow and flight condition.

For purely climbing flight, as schematically depicted in **Figure 12**, $\gamma = \pi/2$, and Eq. (45) reduces to

$$\begin{aligned} P_{M\ \substack{\text{Coandă}-MAV\\\text{Climbing}}\Big|_{\substack{based-on\\\text{Coandă Jet}\\at-hover}}} &= \frac{T_{Coandă-MAV} \bullet \dot{y} - D \bullet \dot{y} - W \bullet \dot{y}}{\left(\text{Coandă } \textit{Jet Rate of} \text{ Momentum Gain} * \text{Coandă } \textit{Jet} \text{ Velocity In}\right)\Big|_{\substack{\text{Coandă Jet}\\at-hover}}} \\ &= \left(\frac{T - (D + W)}{\dot{m} V_{J\text{-}in}}\right)\frac{V}{V_{J\text{-}in}} \end{aligned} \tag{51}$$

Considering the fuel consumed, Eq. (46) becomes

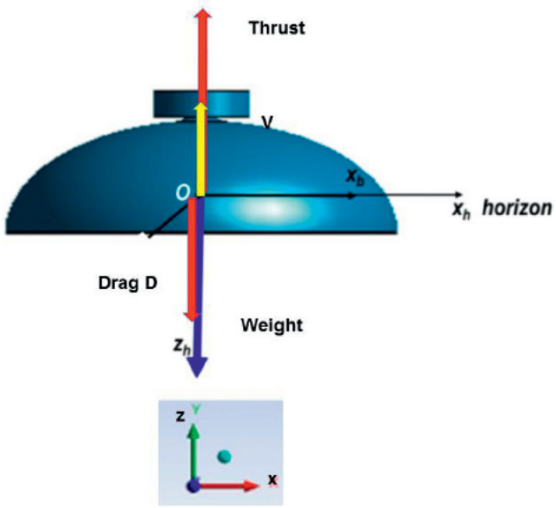

Figure 12. Schematic of Coandă MAV in two-dimensional climb in the vertical plane of symmetry and motion.

$$P_{M\,\substack{\text{Coandă}-MAV\\ \text{Climbing}}}(t)\Big|_{\substack{based-on\\ \text{Coandă Jet}\\ at-hover}} = \frac{T(t)\bullet\dot{y} - D\bullet\dot{y} - \left(W - \int CT(t)dt\right)\bullet\dot{y}}{\left(\text{Coandă Jet Rate of Momentum Gain} * \text{Coandă Jet Velocity In}\right)_{hover}}$$
$$= \left\{\frac{T(t) + \int CT(t)dt}{\dot{m}V_{\substack{J\text{-}in\\ hover}}} - \left(\frac{C_D}{4}\frac{{R_{J-out}}^2}{R_{J-in}h_{J-in}}\left(\frac{V}{V_{\substack{J\text{-}in\\ hover}}}\right)^2 + \left(1 + \ln\frac{R_{J-out}}{R_{J-in}}\right)\right)\right\}\frac{V}{V_{\substack{J\text{-}in\\ hover}}}. \tag{52}$$

If we define that, the thrust T of the Coandă MAV should be able to produce climbing motion for a period of θ seconds, straight forward arithmetic calculation using Eq. (47) will require that the propulsion of the Coandă MAV should have a power capacity exceeding

$$P_{M\,\substack{\text{Coandă}-MAV\\ \text{Climbing}}}(t)\Big|_{\substack{based-on\\ \text{Coandă Jet}\\ at-hover}} = \left\{\left(\Gamma + \frac{\Theta}{7200}\right)\left(1 + \ln\frac{R_{J-out}}{R_{J-in}}\right) - \left(\frac{C_D}{4}\frac{{R_{J-out}}^2}{R_{J-in}h_{J-in}}\left(\frac{V}{V_{\substack{J\text{-}in\\ hover}}}\right)^2\right)\right\}\frac{V}{V_{\substack{J\text{-}in\\ hover}}} \geq 0 \tag{53}$$

corresponding to providing thrust of

$$T_{Coandă-MAV} = \left(2\pi\rho R_{J-in}h_{J-in}V_{J\text{-}in}^2\left(1 + \ln\frac{R_{J-out}}{R_{J-in}}\right)\right)_{hover}(1+\Gamma) \tag{54}$$

where

$$\Gamma \geq \frac{\left(\frac{C_D}{4}\frac{{R_{J-out}}^2}{R_{J-in}h_{J-in}}\left(\frac{V}{V_{\substack{J\text{-}in\\hover}}}\right)^2\right)}{\left(1+\ln\frac{R_{J-out}}{R_{J-in}}\right)} - \frac{CT}{W}\Theta \tag{55}$$

These expressions comprise further development of those given in [31, 33–34]. The Performance Measure $P_{MCoandă\text{-}MAV\ Level\ Flight}$ can be expressed as a function of $C_{D,}R_{o,}\ \dot{m}\ h_{i,}\alpha,\ V,\ V_{J\text{-}in}$. These basic relationships can further be altered to address other flight conditions.

6. Results and examples

6.1. Results and examples for hover

The theoretical prediction for the performance measures P_M as given by Eqs. (41) and (42) are depicted in **Figures. 13–16**. Comparison of the analytical model and the CFD simulation results for another Performance Measure P_{M2} defined as the Coandă MAV lift per Coandă jet inlet velocity as suggested in [11, 29] is shown in **Figure 17** and elaborated in [31, 33–34]. The Performance Measure P_{M2} is calculated for various Jet slot thickness, and serve as an assessment and validation of the theoretical model. Certainly the CFD model for the same Coandă MAV configuration is based on Reynolds averaged Navier-Stokes equations which take into account viscous effects, which is not considered in the theoretical model and analysis. Thus, some discrepancies will appear, and the comparison should be judged as such.

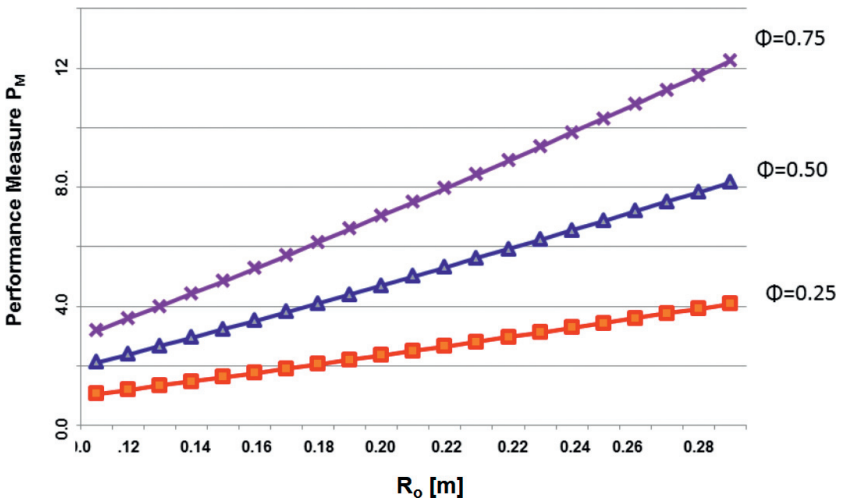

Figure 13. Performance Measure for spherical Coandă MAV for various values of Outer Radius while keeping the Inner Radius R_i and inlet jet slot thickness h_i constant during hover (baseline). In the present example, the Coandă Jet inlet Radius $R_{J\text{-}in}$ = 0.02 m, Coandă jet slot thickness $h_{J\text{-}in}$ = 0.01 m, and Coandă jet inlet velocity $V_{J\text{-}in}$ = 5 m/sec. The performance curves are evaluated at some selected values of mass-flow-Rate Ratio $\Phi_{Coandă-mass} = \frac{\dot{m}_J}{\dot{m}_R}$.

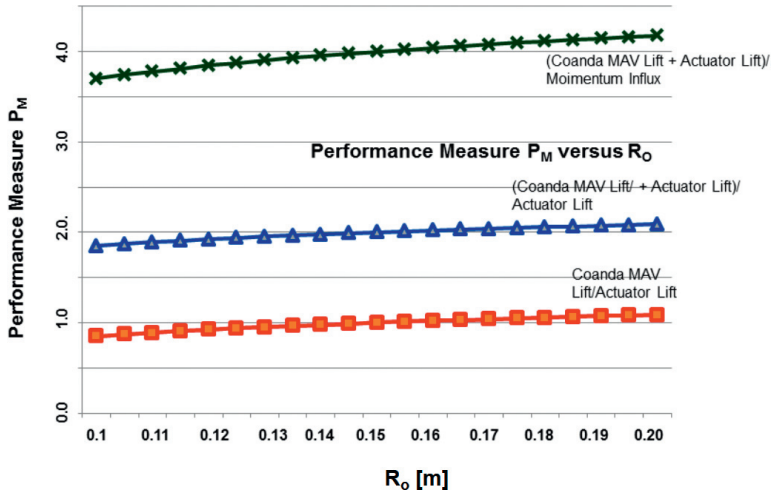

Figure 14. Performance Measure for spherical Coandă MAV for various Outer Radius $R_o[m]$. In the present example, Three different Performance versions are exhibited: Coandă MAV to Actuator Lift Ratio, Combined Coandă MAV and Actuator to Actuator lift Ratio, and Combined Coandă MAV and Actuator to Momentum Rate Ratio. Coandă Jet inlet Radius $R_{J\text{-}in} = 0.02$ m, Coandă jet slot thickness $h_{J\text{-}in} = 0.01$ m, and Coandă jet inlet velocity $V_{J\text{-}in} = 5$m/sec.

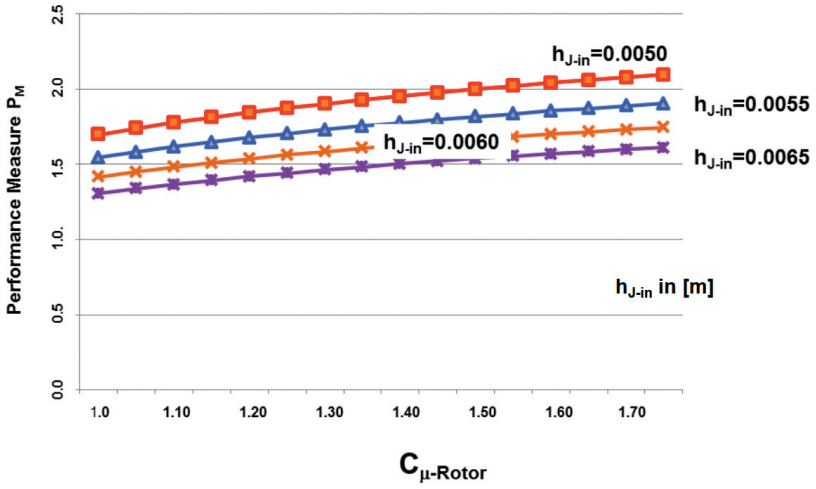

Figure 15. Performance Measure for spherical Coandă MAV as a function of Coandă jet Momentum Coefficient C_μ for various values of $h_{J\text{-}in}$. Similar to **Figure 15**, here the Coandă Jet inlet Radius $R_{J\text{-}in} = 0.02$ m, Coandă jet slot thickness $h_{J\text{-}in} = 0.01$ m, and Coandă jet inlet velocity $V_{J\text{-}in} = 5$ m/sec have been used as the baseline.

Comparison of analytical and CFD [32] models for the Performance Measure P_{M2} defined by total lift L_{MAV}/ Inlet Velocity $V_{j\text{-}in}$ for spherical Coandă is depicted in **Figure 17**. The figure clearly exhibits the noticeable influence of the ratio of the jet slot thickness h to the reference radius R_o, to the Performance Measure P_{M2}. The influence of the jet inlet velocity on lift enables designers to appropriately select the right propulsion system specifications for the Coandă MAV.

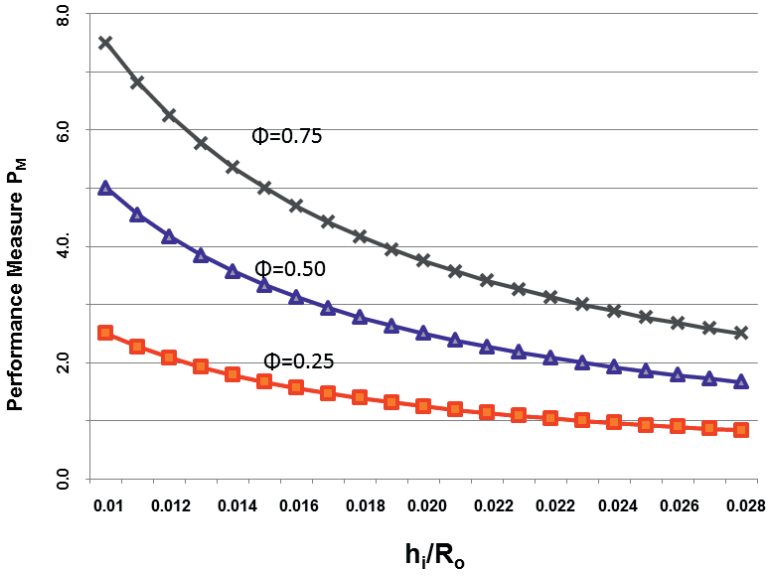

Figure 16. Performance Measure for spherical Coandă MAV as a function of $h_{J\text{-}in}$ /R_o for various values of Coandă jet mass-flow-Rate Ratio $\Phi_{Coandă-mass} = \frac{\dot{m}_J}{\dot{m}_R}$. Similar to **Figure 15**, here the Coandă Jet inlet Radius $R_{J\text{-}i\ n} = 0.02$m, Coandă jet slot thickness $h_{J\text{-}in}$=0.01m, and Coandă jet inlet velocity $V_{J\text{-}in}$=5m/sec.

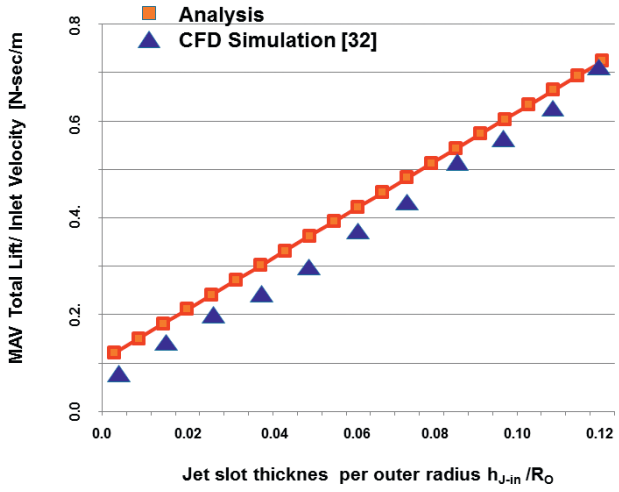

Figure 17. Analytical and CFD [32] models comparison Total Lift L_{MAV}/Inlet Velocity $V_{j\text{-}in}$ for spherical Coandă MAV for various Jet slot thickness $h_{j\text{-}in}$ per outer radius R_o.

Figure 18 exemplifies the effect of viscosity for two different locations of the Coandă jet introduction that can be revealed by CFD simulation. The CFD images in **Figure 18 (a)** and **(b)**, which simulate the velocity magnitude contours for similar configurations considered by Mirkov and Rasuo [11, 29] and Ghozali [30], show the velocity magnitude contours for each of these configurations and exhibit the influence of the inlet configuration. The resulting lift as a function of input jet velocity diagram for each of these configurations are also shown. The corresponding computational grid for each of the configurations utilized by Mirkov and Rasuo, and Ghozali, is also shown as inset in each figure.

For these CFD simulations, which were performed using steady RANS (Reynolds Averaged Navier-Stokes), two equations k-ω shear stress transport (SST) turbulence model is employed. In the solution procedure followed, simple pressure-velocity coupling scheme with the least squares cell base as discretization gradient has been applied; second order upwind for the momentum equation and the turbulent kinetic energy were also imposed.

Figure 18 also exhibits structured numerical mesh used in the flow domain. Through meticulous attempts and grid sensitivity studies the size of the mesh cells was generated small to enable visualizations of the flow around the whole body with best details. The CFD simulations are carried out on two configuration versions: in **Figure 18 (a)**, the flow configuration and grid mesh are closely similar to those utilized by Mirkov and Rasuo [11, 29], and in **Figure 18 (b)**, the flow configuration and grid mesh are closely similar to those utilized by Ghozali [30]. The inset of each figure shows the mesh details adopted by Mirkov and Rasuo [29], and Ghozali [30], respectively. Moderately small Reynolds number, $Re = 68458$, based on mean velocity and jet inlet height has been employed in the numerical study. Additionally, across the inlet which has a thickness of 0.05 m, the velocity is st to be uniform ($V_{j\text{-}in} = 20$ m/s). The CFD simulations utilize computational grid with 52,830 mesh cells. Assessment of the results and referring to the procedure guidelines assure that the mesh quality was acceptable. The CFD computational results indicate that orthogonality quality was 4.96943e-01. Again, from the ANSYS orthogonality quality requirements, these figures should be acceptable. Further details are elaborated by Djojodihardjo et al. [31, 32–35] and Ahmed et al. [33, 34–36].

Grid sensitivity [18–19] and iteration convergence CFD simulation [44] studies were carried out and exhibited in **Figure 19**. The mesh quality and comparable agreements between the present CFD simulation results exhibited in **Figure 18**, as well as the supporting grid mesh and convergence studies exemplified by **Figure 19** demonstrates that the generation of mesh in the present CFD simulations meet the present quality requirements as well as those stipulated in the ANSYS™© guidelines; therefore these can be considered to be acceptable.

The CFD simulations are also carried out to investigate the influence of the jet inlet radius on the air vehicle performance (lift). The CFD simulations were carried out for two inlet jet radius, $R_i = 5$ mm and $R_i = 50$ mm for the baseline semi-spherical Coandă MAV configurations studied. The results are presented as velocity magnitude contours, which exhibit the influence of the inlet radius on the flow field. **Figures 20** and **21** exhibits the pressure contours along semi-spherical Coandă MAV surface obtained by CFD simulation results and the static pressure associated with it in color-coded contour. **Figure 22** compares the CFD simulation results for the pressure coefficient of on the Coandă MAV surface jet blanket obtained from the

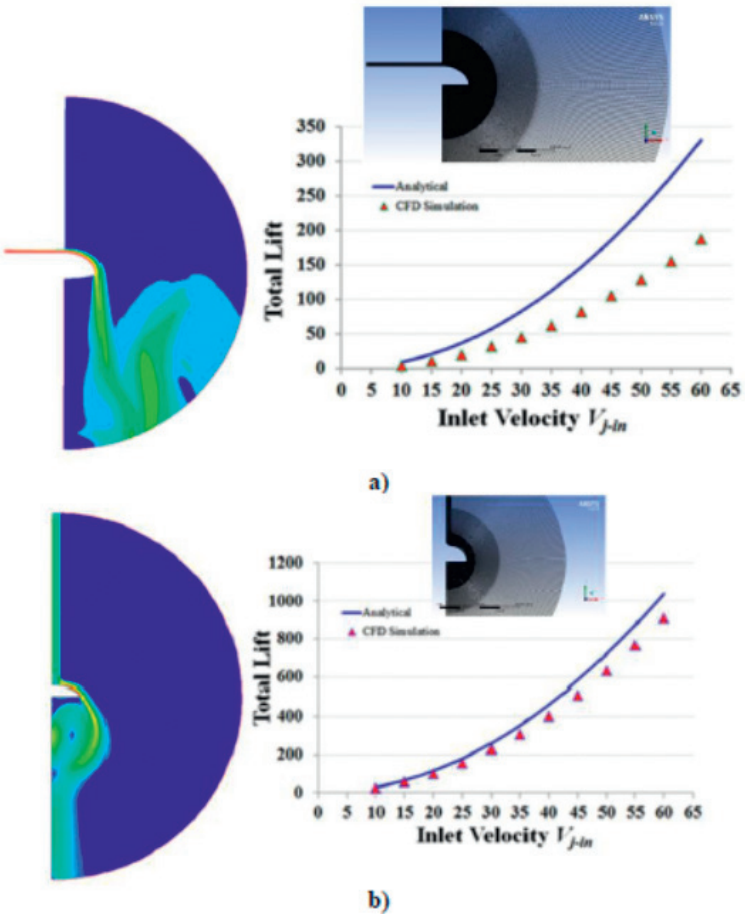

Figure 18. Lift versus input jet velocity for similar configuration considered in (a) Mirkov and Rasuo [11, 29], (b) Ghozali [30]. The inset of each figure show the mesh details adopted by Mirkov and Rasuo [29], and Ghozali [30], respectively, that have been reproduced in the present CFD simulations.

present CFD simulation and those obtained by Mirkov and Rasuo [29]. Overall, these results serve to verify the plausibility of the analytical as well as the CFD simulation efforts.

6.2. Results and examples for translation

For translatory flight, some examples of Performance Measures simulation studies for Coandă MAV in purely level are exhibited by **Figures 23** and **24**, obtained using Eqs. (44) and (48), respectively.

Figure 23 is worked out for the Coandă Jet inlet Radius $R_{J\text{-}in} = 0.02$ m, Coandă jet slot thickness $h_{J\text{-}In} = 0.01$ m, and Coandă jet inlet velocity $V_{J\text{-}n} = 5$ m/sec.. **Figure 24** shows the Thrust ratio Γ as a function of versus flight velocity for pure climbing, following Eq. (49) with equal sign,

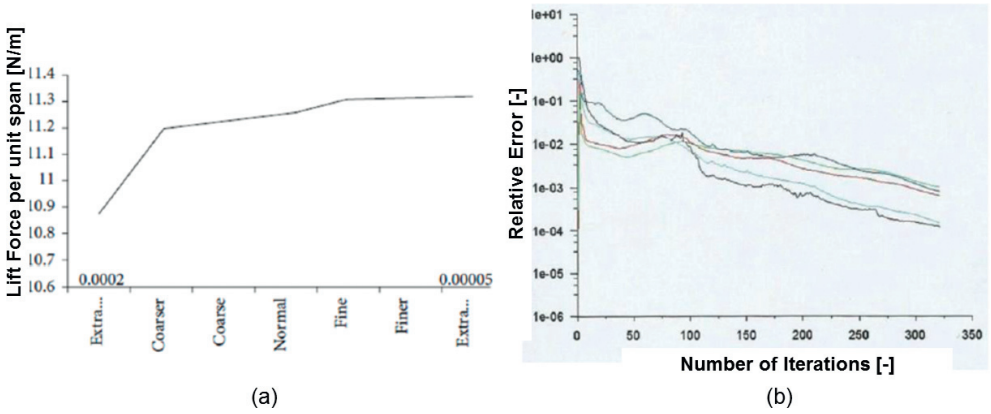

Figure 19. (a) Two-dimensional CFD grid sensitivity study for lift force per unit span on an airfoil at 0° angle of attack [18–19]; (b) Iteration Convergence CFD simulation studies [44]. Both are carried out using ANSYS® [45]. The curves are untouched computer outputs.

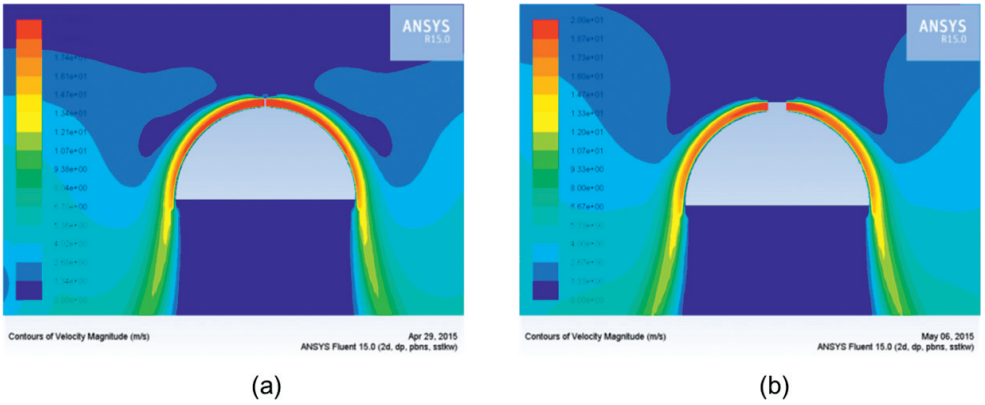

Figure 20. CFD simulation on two Coandă MAV configurations (a) *Ri*=5 mm, (b) $R_i = 50$ mm. Relatively symmetrical Coandă effect velocity magnitude contours are exhibited. The images are untouched computer outputs.

assuming $C_D \approx 2.0$ and specific fuel consumption $C = 0.000139$ and period = 1 h. The example is also worked out for the Coandă Jet inlet Radius $R_{J\text{-}in} = 0.02$ m, Coandă jet slot thickness $h_{J\text{-}in} = 0.01$ m, and Coandă jet inlet velocity $V_{J\text{-}in} = 5$ m/sec.

Parametric study results exhibited by these figures can be utilized to give insight on the performance of the semi-spherical Coandă MAV considered as well as for preliminary sizing purposes.

7. Concluding remarks

A comprehensive and meticulous analysis has been made to analyze the potential utilization of Coandă MAV as an aerial robotic platform (vehicle) and deriving the Coandă MAV

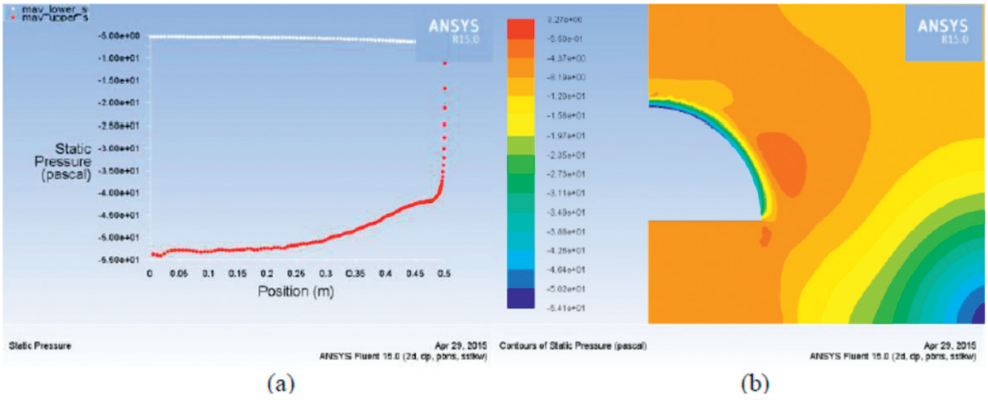

Figure 21. CFD simulation results plot of surface static pressure (a) and flow field pressure contours image (b) for the baseline semi-spherical Coandă MAV. The images are untouched computer outputs.

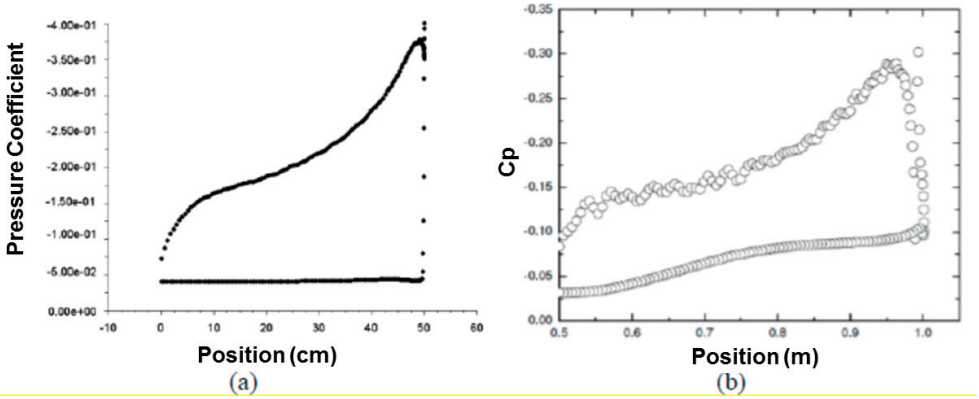

Figure 22. CFD computational results comparison of the surface pressure coefficient on the Coandă MAV jet blanket; (a) presents CFD simulation results and (b) Mirkov and Rasuo CFD simulation results [11, 29]. The images are untouched computer outputs.

governing equations. Utilizing first principles, i.e., conservation principles for control volume analysis as baseline fluid-dynamic analysis for the Coandă MAV in hover and free-body diagram and Newton's law of motion as baseline flight-dynamic analysis for in-plane translatory motion, the analysis establishes the basic working relationships among various relevant variables and parameters governing the aerodynamics forces and performance measures of Coandă MAV in hover and translatory motion.

To gain insight in the development of the analytical model, and to assess and validate the analytical model subject to the theoretical assumptions, CFD simulations for the Coandă MAV generic models are carried out. Comparison of the theoretical analysis and CFD simulation

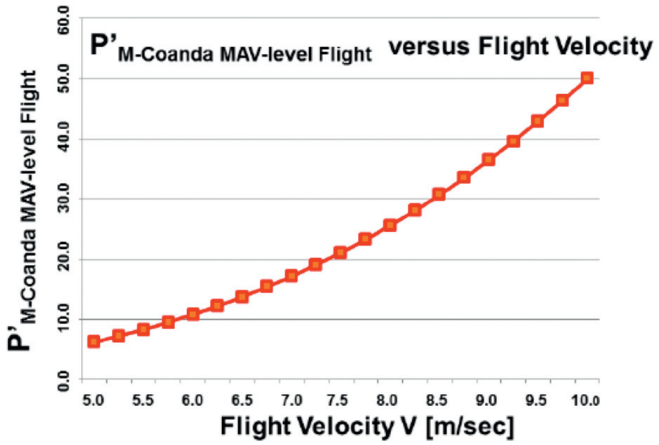

Figure 23. Coandă MAV Performance Measure for level flight as a function of flight velocity as defined by Eq. (44a). The example is worked out for the Coandă Jet inlet Radius $R_{J\text{-}in} = 0.02$ m, Coandă jet slot thickness $h_{J\text{-}in} = 0.01$ m, and Coandă jet inlet velocity $V_{J\text{-}in} = 5$ m/sec.

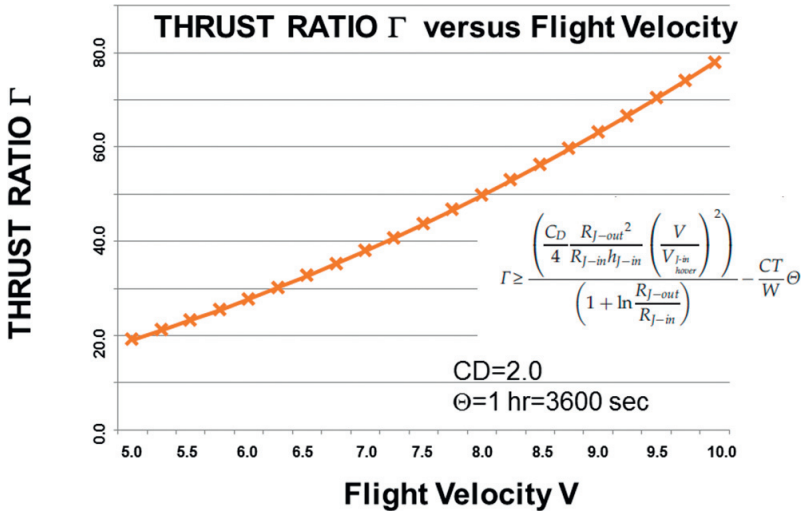

Figure 24. Thrust Ratio Γ as a function of versus flight velocity for pure climbing, following Eq. (49) with equal sign, assuming C ≈ 2.0 and Specific Fuel Consumption C = 0.000139 and period = 1 h. The example is also worked out for the Coandă Jet inlet Radius $R_{J\text{-}in} = 0.02$ m, Coandă jet slot thickness $h_{J\text{-}in} = 0.01$ m, and Coandă jet inlet velocity $V_{J\text{-}in} =$ 5 m/sec.

results indicates the plausibility of the theoretical approach. Performance measures are derived to elaborate the significance of Coandă jet momentum coefficient and to assess the effectiveness of the Coandă MAV as an aerial robot platform.

Author details

Harijono Djojodihardjo

Address all correspondence to: harijono@djojodihardjo.com

The Institute for the Advancement of Aerospace Science and Technology, Jakarta, Indonesia

References

[1] Coandă H. Procédé et dispositif pour faire dévier une veine de fluide pénétrant dans un autre fluide. Brevet d'invention France. 1934

[2] Coandă H, France C. Device for Deflecting a Stream of Elastic Fluid Projected into an Elastic Fluid. US Patent Office, 2,052,869, 1936, ed.: Google Patents

[3] Gad-el-Hak M. Flow Control - Passive, Active and Reactive Flow Management. London: Cambridge University Press; 2000

[4] Liu Y, Sankar LN, Englar RJ, Ahuja KK. Numerical Simulations of the Steady and Unsteady Aerodynamic Characteristics of a Circulation Control Wing Airfoil AIAA Paper 2001-0704; 2001

[5] Kweder J, Panther C, Smith JE. Applications of circulation control, yesterday and today. International Journal of Engineering (IJE). 2011;4(5):411-429

[6] Englar RJ. Development of the A-6/Circulation Control Wing Flight Demonstrator Configuration. Defense Technical Information Center, Document. 1979

[7] Pugliese A, Englar RJ. Flight Testing the Circulation Control Wing. New York, N. Y: American Institute of Aeronautics and Astronautics, Aircraft Systems and Technology Meeting; 1979

[8] Mamou M, Khalid M. Steady and unsteady flow simulation of a combined jet flap and Coandă jet effects on a 2D airfoil aerodynamic performance. Revue des Energies Renouvelables CER'07 Oujda. 2007; 55-60

[9] Englar RJ, Hemmerly RA, Taylor DW, Moore WH, Seredinsky V, Walter W. Design of the circulation control wing STOL demonstrator aircraft. Journal of Aircraft. 1981;18:51-58

[10] Schroijen N, van Tooren M. MAV Propulsion System using the Coandă Effect. American Institute of Aeronautics and Astronautics. 45th AIAA/ASAME/SAE/ASEE. Exhibit. Joint Propulsion Conference, Denver, Colorado. 2009. pp. 1-10

[11] Mirkov N, Rasuo B. Numerical simulation of air jet attachment to convex walls and applications. International Congress of the Aeronautical Sciences; 2010. pp. 1-7

[12] Rumsey CL, Nishino T. Numerical study comparing RANS and LES approaches on a circulation control airfoil. International Journal of Heat and Fluid Flow. 2011;32:847-864

[13] Radespiel R, Burnazzi M. Fundamentals in Coandă Flap Design. Berlin Heidelberg: Springer-Verlag; 2011. https://www.researchgate.net/profile/Rolf_Radespiel/publication/283231590_Fundamentals_in_Coandă_Flap_Design/links/5698e9d108ae34f3cf207911/Fundamentals-in-Coandă-Flap-Design.pdf [Accessed: June 15, 2014]

[14] Djojodihardjo H. Progress and development of Coandă jet and vortex cell for aerodynamic surface circulation control – An overview. The SIJ Transactions on Advances in Space Research & Earth Exploration (ASREE). September-October 2013;1(1):32-42

[15] Djojodihardjo H, Thangarajah N. Research, development and recent patents on aerodynamic surface circulation control-A critical review. Recent Patents on Mechanical Engineering. 2014;7:1-37

[16] Tongchitpakdee C, Benjanirat S, Sankar LN. Numerical studies of the effects of active and passive circulation enhancement concepts on wind turbine performance. Journal of Solar Energy Engineering. 2006;128(4):31023089

[17] Tongchitpakdee C. Computational studies of the effects of active and passive circulation enhancement concepts on wind turbine performance [PhD Thesis]. Georgia Institute of Technology; 2007. https://www.scribd.com/document/38534330/Chanins-Thesis [Accessed 15 July 2015]

[18] Abdul-Hamid MF, Djojodihardjo H, Suzuki S, Mustapha F. Numerical assessment of Coandă effect as airfoil lift enhancer in wind-turbine configuration. In: Regional Conference on Mechanical and Aerospace Technology; 9-10 February 2010; Bali

[19] Djojodihardjo H, Abd Hamid MF, Basri S, Romli FI, Abdul Majid DLA. Numerical simulation and analysis of Coandă effect circulation control for wind-turbine application considerations. IIUM Engineering Journal, Special Issue, Mechanical Engineering. 2011. pp 19-42

[20] Djojodihardjo H, Abdul-Hamid MF, Jaafar A, Basri S, Romli FI, Mustapha F, Mohd-Rafie AS, Abdul-Majid. Computational study on the aerodynamic performance of wind turbine airfoil fitted with Coandă jet. Journal of Renewable Energy, Hindawi Publishing Co. 2013;2013:17, Article ID 839319, http://dx.doi.org/10.1155/2013/839319

[21] Erath B, Plesniak MW. The occurrence of the Coandă effect in pulsatile flow through static models of the human vocal folds. Journal of the Acoustical Society of America. August 2006;120(2):1000-1011

[22] Zheng X, Mittal R, Bielamowicz S. A computational study of asymmetric glottal jet deflection during phonation. Journal of the Acoustical Society of America. 2011;129(4):2133-2143

[23] Scheinherr A. Glottal motion and its impact on airflow and aerosol deposition in upper airways during human breathing [PhD Thesis]. Institut de Recherchesur les Phénomènes Hors Équilibre, Ecole Centrale du Marseille; 2015. https://hal.archives-ouvertes.fr/tel-01169649/document [Accessed 15 July 2015]

[24] Djojodihardjo H, Ahmed RI. CFD simulation of Coandă effect on the upper respiratory system. Journal of Medical Imaging and Health Informatic. October 2016;6(6):1526-1535(10)

[25] Prandtl L. Über Flüssigkeitsbewegung bei sehr kleiner Reibung Int. Math. Kongr. Heidelberg. Leipzig; 1904

[26] Frank A, McGrewy JS, Valentiz M, Levinex D, How JP. Hover, Transition, and Level Flight Control Michelson, C. Test and evaluation for fully autonomous micro air vehicles. ITEA Journal. 2008;29(4):1-12. Available from: http://citeseerx.ist. psu.edu/viewdoc/download?doi¼10.1.1.212.6553&rep¼rep1&type¼pdf [Accessed: April 30, 2015]

[27] Dumitrache A, Frunzulica F, Ionescu TC. Mathematical modelling and numerical investigations on the Coandă effect, Dumitrache et al. InTech; 2012. http://dx.doi.org/10.5772/50403 [Accessed: June 15, 2013]

[28] Constantinescu SG, Niculescu ML. Experimental and numerical research of lift force produced by Coandă effect. AIP Conference Proceedings. 2013;1558:152. DOI: 10.1063/1.4825443

[29] Mirkov N, Rasuo B. Maneuverability,of a UAV with Coandă Effect Based Lift Production. International Congress of the Aeronautical Sciences; 2012. pp. 1-6

[30] Ghozali D. Analysis of Coandă effect using computational-fluid-dynamic [Thesis]. Indonesia: Universitas Gajah Mada; 2013

[31] Djojodihardjo H, Ahmed RI. An analysis on the lift generation for Coandă micro air vehicles. In: IEEE, ICARES Conference Proceeding; Yogyakarta; 2014

[32] Djojodihardjo H, Ahmed RI, Abu-Thalib AR, Mohd-Rafie AS. Analytical and CFD visualization studies of Coandă MAV, In: Proceedings, The 13th Asian Symposium on Visualization; 22-26 June 2015; Novosibirsk, Russia. Russian Academy of Sciences and Kristianovich Institute of Theoretical and Applied Mechanics

[33] Ahmed RI, Djojodihardjo H, Abu-Talib AR, Abd-Hamid MF. Application of Coandă jet for generating lift of micro air vehicles - Preliminary design considerations. Applied Mechanics and Materials. 2014;629:139-144

[34] Ahmed RI, Djojodihardjo H, Abu-Talib AR, Mohd-Rafie AS. First principle analysis of Coandă micro air vehicle aerodynamic forces for preliminary sizing. Aircraft Engineering and Aerospace Technology. 2016;89(2):231-245. DOI: 10.1108/AEAT-03-2015-0080

[35] Djojodihardjo H, Ahmed RI. Basic Coandă MAV fluid dynamics and flight mechanics, Fifteenth Asian Congress of Fluid Mechanics (15ACFM) IOP Conference Series Journal of Physics: Conference Series 822, 012051, 2017

[36] Ahmed RI, Abu-Talib AR, Mohd-Rafie AS, Djojodihardjo H. Aerodynamics and flight mechanics of MAV based on Coandă effect. Aerospace Science and Technology. March 2017;62:136-147

[37] Davis Jr. WR, Kosicki B, Boroson DM, Kostishack DF. Micro air vehicles for optical surveillance. The Lincoln Laboratory Journal, MIT. 1996;9(2):197-214

[38] Poisson-Quinton Ph, Lepage L. Survey of French research on the control of boundary layer and circulation. In: Lachmann GV, editor. Boundary Layer and Flow Control: Its Principles and Application. Vol. 1. New York: Pergamon Press; 1961. pp. 21-73

[39] Van Kuik GAM. The relationship between loads and power of a rotor and an actuator disc. Journal of Physics: Conference Series. 2014;555:012101

[40] Bangura M, Melega M, Naldi R, Mahony R. Aerodynamics of Rotor Blades for Quadrotors, arXiv:1601.00733v1 [physics.flu-dyn] [Internet]. 5 January 2016. Available from: https://arxiv.org/pdf/1601.00733.pdf [Accessed: April15, 2017]

[41] Anonymous. Froudes' Momentum Theory: (Actuator Disk Theory). Available from: 17 http://www.public.iastate.edu /_aero442/unit2.pdf [Accessed: April 15, 2017]

[42] Anonymous. Froudes' Momentum Theory: (Actuator Disk Theory). Available from: http://www.public.iastate.edu /∼aero442/unit2.pdf [Accessed: April 15, 2017]

[43] Betz A. Das Maximum der theoretisch moeglichen Ausnuetzung des Windes durch Windmotoren. Zeitschrift für das gesamte Turbinenwesen, 26, 307-309. (In German)

[44] Ahmed RI. Theoretical foundation and numerical analysis on Coandă Effect for micro-air vehicle [PhD Thesis]. Universiti Putra Malaysia; 2016

[45] Anonymous. ANSYS® ICEM CFD Tutorial Manual. Available from: 148.204.81.206/Ansys/150/ANSYS%20ICEM%20 CFD%20 Tutorial%20Manual.pdf [Accessed: January 15, 2011]